Downloaded 09/20/16 to 95.215.237.244. Redistribution subject to SEG license or copyright; see Terms of Use at http://library.seg.org/

Joint inversion of water velocity and node position for ocean bottom node data

Amir Amini[*], *Hao Peng, Zhao Zhang, Rongxin Huang, and Jing Yang*

Summary

Variation of sound wave velocity in water (water velocity) and node positioning errors can cause strong 4D noise in ocean bottom node (OBN) time-lapse processing if they are not addressed correctly. Here we proposed a method to jointly invert the water velocity and the node position from the recorded direct arrival time in the data. We validated this method using synthetic and real OBN data examples from deep-water Gulf of Mexico.

Introduction

Excellent shot and receiver position repeatability of OBN acquisitions in conjunction with the relatively quiet recording environment make OBN surveys an ideal candidate for deep-water reservoir monitoring. The good repeatability of node positioning is achieved by utilizing a Remotely Operated Vehicle (ROV) to deploy nodes in designated locations at the water bottom. However, due to the accuracy limit of the inertial guidance system that the ROV employs to measure its own positioning, an uncertainty on the order of a few meters can exist between the actual positions of the nodes and their positions recorded by the ROV during deployment. If incorrect positions of nodes are used for migration of the data, 4D noise can occur.

Another significant source of 4D noise comes from the changes of water column conditions during/between base and monitor surveys, e.g., changes of water column thickness due to tidal cycles, or changes of water velocity due to variations of temperature, pressure, and salinity in the sea water. In deep-water Gulf of Mexico (GoM), where tidal changes are relatively small, water velocity variation is the main contributor to the water column statics errors, especially for the down-going wavefield which travels through the water column three times. Correction of water column statics on seismic data requires *a priori* knowledge of the actual water velocity during surveys. Recently, an instrument called pressure inverted echo sounder (PIES) (Wang et al., 2012) was developed and used to estimate the average water velocity by measuring the depth-dependent pressure and the two-way flight time. However, the measurements from PIES are restricted to the specific location and depth at which they are planted and inaccuracies can exist in the measured velocity due to the uncertainty in the pressure-to-depth conversion.

Most previous work has focused on extracting water velocity information from the recorded direct arrival time in the data (e.g. Dosso et al., 1998). Since the direct arrival time is dependent on the distance between node and shot positions as well as the water velocity, these two quantities are strongly correlated and need to be inverted jointly (Lecerf et al., 2011). Joint inversion of water velocity and node position had been proposed in a number of studies previously (Undengaard and Craft, 2012; Ahmed et al., 2013). However, their methods used a straight ray approximation to compute the direct travel time, which may incur systematic errors when the water velocity varies with depth significantly. Stopin et al. (2011) employed ray-tracing in their computation of direct arrival time, but node positions might not have been jointly inverted with other quantities in their study.

In this paper, we propose a method to jointly invert the water velocity and node position by taking advantage of the ray-traced direct arrival times. In order to use the data from all nodes regardless of their depth, we used a two-layer model. We tested the validity of our inversion results with analysis of synthetic and 4D real data examples.

Methodology

In general, the velocity of sound waves in the ocean depends on temperature, pressure (or depth), and salinity. Therefore, water velocity may be considered to vary with time of the year and water depth (salinity plays a much weaker role). Assuming that water velocity does not vary with horizontal position, the travel time T for each shot-node pair, can be expressed as:

$$T = \int_s^r \frac{dl}{v(z,t)}, \quad (1)$$

where $v(z,t)$ is the interval water velocity which depends on water depth z and acquisition time t and dl is the differential ray length between shot (s) and node (r) locations.

In the shallow thermocline region, velocity changes with both temperature and depth, whereas in the deep, where water temperature is nearly constant, it effectively changes with depth only. Consequently, in deep water the velocity change with acquisition time is not the same for the entire water column. To incorporate the difference between shallow and deep regions of water column, we adopted a two-layer scaled Hood function water velocity model (Advocate and Hood, 1993) with the following parameterization for interval velocity (see Zietal and Haacke, 2016, for a similar parametrization):

$$v(z,t) = \begin{cases} s(t)\, v_h(z) & z \le z_o \\ s_o\, v_h(z) & z > z_o \end{cases}, \quad (2)$$

© 2016 SEG

Downloaded 09/20/16 to 95.215.237.244. Redistribution subject to SEG license or copyright; see Terms of Use at http://library.seg.org/

where v_h is the GoM Hood function water velocity profile. $s(t)$ and s_o are scalars for the shallow and deep layer, respectively. z_o is the depth where the shallow water column roughly transitions to deep (1200~1300 m for GoM). We set z_o =1250 m in what follows. The scalars $s(t)$ and s_o are later obtained by inversion.

The travel time T, calculated by ray tracing based on the interval velocity profile, can deviate from the direct arrival time T_{pick} picked from data, due to water velocity and node positioning errors. The picked and computed direct arrival time misfit dT, for each shot-node pair has the following functional form:

$$dT := T - T_{pick} = f(X, Y, Z, s(t), s_o), \quad (3)$$

where X, Y, Z are node position coordinates. The constant scalar s_o and $s(t)$ are the scalars for deep and shallow layer velocities. Here we assume node clock drift, the other important factor affecting the direct arrival time (Olofsson and Woje, 2010), has been corrected in the input data using time stamps from deployment and retrieval or using other means such as seismic interferometry with passive seismic data (Hatchel and Mehta, 2010).

In the current method, we use the alternating-direction iterative method (Peng and Li, 2010) to solve this highly nonlinear problem and invert water velocity and node X/Y/Z alternately while invoking the appropriate geometrical and physical constraints on each quantity during iterations. Terms more sensitive to dT such as water velocity are solved first, followed by others in each iteration.

Synthetic data example

To validate our method, we constructed synthetic data with a maximum offset of 3 km based on the Atlantis 2014-2015 OBN survey acquired by Fairfield Nodal. This survey was acquired with ~1900 nodes spaced 369-426 m apart and arranged in a honeycomb (hexagonal) pattern. The area straddles the Sigsbee Escarpment, and the sea floor beneath the nodes drops from 1270 m to 2200 m. Shots were fired every 16 seconds during the acquisition period of 80 days. Shot-node pairs with near offsets up to 3 km were selected for inversion (about 21 million traces). To generate velocity variation with shooting time, the shallow layer velocity was perturbed from the background GoM profile by adding two sinusoidal functions of periods of 1 day and 80 days to mimic seasonal and daily water velocity changes. The deep-water velocity was kept the same as the GoM water velocity. Node position was then modified from its initial "field" values, in each of x, y, and z directions by random magnitudes within the +/- 3 m range.

Figure 1 shows the shallow-layer inverted average water velocity $\langle s(t)v_h \rangle$ compared to the actual velocity. Except at the boundaries (beginning and end of shooting), where the number of data points available for inversion was statistically sparse, the inverted velocity matched the actual velocity quite well. The gaps in the inverted results were due to the absence of recorded (less than 3 km offset) data points for some acquisition time periods. Comparing Figures 2a through 2i, we observe that the imposed perturbations in node positions were adequately recovered after inversion. Figure 3 illustrates how dT maps for a few neighboring nodes of synthetic data improved as water velocity, node X/Y position, and node depth (Z) were progressively corrected. Each node, with shots within a 3 km offset range, was depicted by a disk with the node at its

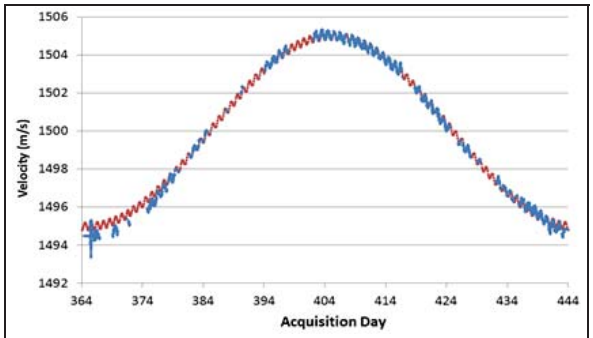

Figure 1: Inverted shallow-layer (0 to 1250 m) average water velocity $\langle s(t)v_h \rangle$ for synthetic data (blue symbols). Red symbols are actual shallow-layer velocities.

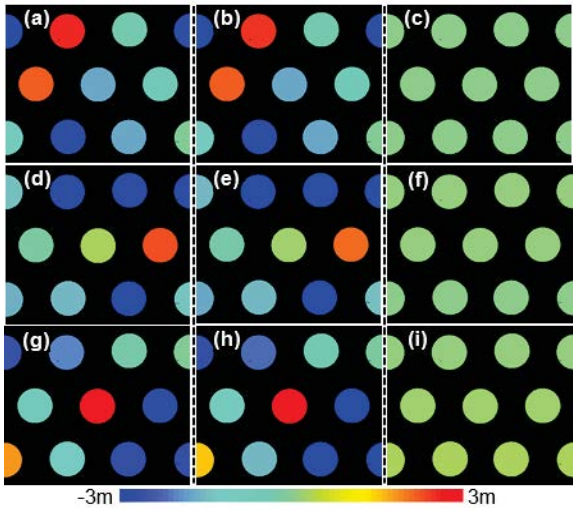

Figure 2: Node X/Y/Z position inversion results for synthetic data example; (a – c): actual node x perturbation, inverted node x perturbation, difference between actual and inverted node x perturbation. (d – f): actual node y perturbation, inverted node y perturbation, difference between actual and inverted node y perturbation. (g – i): actual node depth perturbation, inverted node depth perturbation, difference between actual and inverted node depth perturbation. Each circle represents a node.

© 2016 SEG

Downloaded 09/20/16 to 95.215.237.244. Redistribution subject to SEG license or copyright; see Terms of Use at http://library.seg.org/

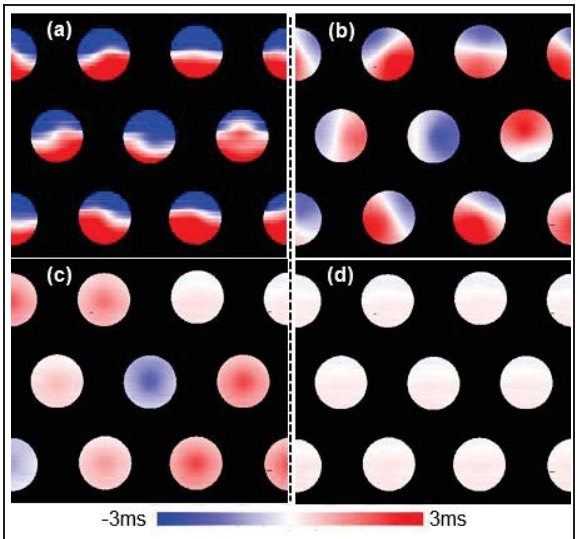

Figure 3: *dT* map of a few neighboring nodes for synthetic data example; (a) before inversion, (b) after water velocity correction, (c) after water velocity and node X/Y position corrections, (d) after water velocity, node X/Y position, and node depth corrections. Each disk represents a node located at the center of the disk and the shots within a 3km offset range.

center. Note that *dT* misfits of less than +/-1 ms were obtained after the last step (Figure 3d).

Inversion results on 4D real data

Here, we describe the inversion results pertaining to a time-lapse survey in deep-water Gulf of Mexico. To pick the direct arrival from the down-going wavefield, designature was performed first to zero phase the data. This not only allowed us to pick more reliably but also moved the source datum to mean sea level. To avoid picking direct arrival wavelets obscured by refractions, we limited the data used for the inversion to offsets less than 3km.

Next, two iterations of inversion were performed separately on the baseline and monitor surveys to invert the actual water velocity and node X/Y/Z position. The average velocity of the shallow section, $\langle s(t)v_h \rangle$, for the monitor survey is plotted in Figure 4 as a function of acquisition day. The gaps in the inverted results were later filled by interpolation from neighboring shots close in time. For this survey, PIES units planted on the seafloor at different depths measured the pressure (converted to depth) and flight time of transmitted high-frequency signals traveling through the water column. The inverted velocity captured the trend obtained by the PIES unit. The discrepancy in the values, however, can be partly attributed to uncertainties in PIES pressure-to-depth conversion and/or potential errors in the inversion. Inverted velocities found individually for base and monitor surveys are plotted in Figure 5a. Figures 5b through d show the *dT* map for a few neighboring nodes

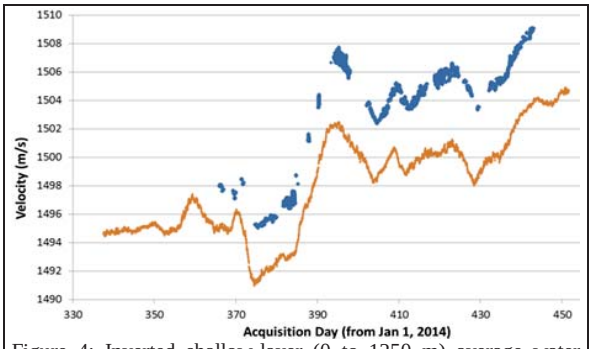

Figure 4: Inverted shallow-layer (0 to 1250 m) average water velocity $\langle s(t)v_h \rangle$ for 2015 survey (blue symbols). Orange symbols are shallow-layer (0 to 1250 m) average velocities extracted from measurement of pressure and flight time by a PIES unit planted at ~ 1328 m depth.

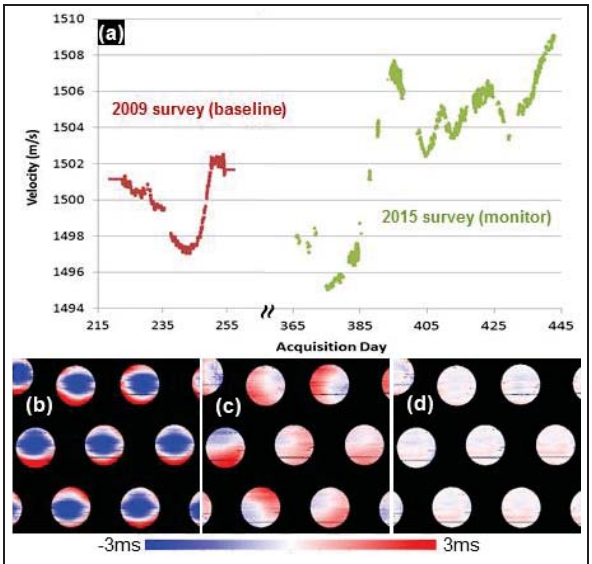

Figure 5: (a) Inverted shallow-layer (0 to 1250m) RMS water velocity $\langle s(t)v_h \rangle$ for baseline (red), and monitor (green) surveys. Acquisition day origin for each survey is Jan 1 of the year in which that acquisition started. (b – d) *dT* map of a few neighboring nodes from the monitor survey; (b) before inversion, (c) after water velocity correction, (d) after water velocity and node X/Y/Z position corrections.

of the monitor survey after inversion, as water velocity and node positions are progressively inverted. Similar to the synthetic data example, *dT* dropped to less than +/-1ms after the last step. A striped pattern observed on the maps before inversion, provided it was shared among all nodes, indicated velocity errors. The inverted constant, s_o, was determined to be 0.9985 for the baseline and 1 for the monitor survey.

To apply the inversion results, we first corrected the node positions by updating their x/y/z values from inversion.

© 2016 SEG

Downloaded 09/20/16 to 95.215.237.244. Redistribution subject to SEG license or copyright; see Terms of Use at http://library.seg.org/

Then, the effect of the changing water column velocity was corrected in an angle-dependent fashion (one time shift at each sample at each trace). Because of the presence of complex subsurface structures, e.g., a steeply dipping water bottom and shallow salt fingers associated with the Sigsbee escarpment, the angle-dependent water-velocity correction was done through the sparse Tau-P inversion method that is less affected by complex geology (Huang et al., 2016).

To examine the impact of inversion on the images and their 4D difference, we migrated the baseline and monitor data using a 25 Hz reverse-time migration (RTM). The top row of Figure 6 displays stacked sections of the 4D difference without inversion, with inversion but excluding node depth, and with inversion including node depth. Figure 6e shows less 4D noise than Figures 6a and 6c since sedimentary layers in the overburden area (above the target reservoir) were better aligned between the two surveys. The bottom row of Figure 6 displays the corresponding 4D NRMS (Normalized Root Mean Square) repeatability measure extracted from the water bottom event. Note that with water-velocity and node position inversion, the 4D NRMS values were significantly reduced. In fact, they dropped to less than 0.1 (or 10%) in most locations inside the node coverage area.

Conclusions and discussions

The two-layer water velocity model described in this work allows for integration of all node data irrespective of their depths. The use of ray tracing improves the accuracy of the computed theoretical direct arrival time. Incorporating these two, the current water velocity and node position joint inversion resulted in residual travel time errors less than +/- 1 ms for the majority of data points in both synthetic and real data examples, making it suitable for 4D applications. The validity of the proposed inversion method was demonstrated through synthetic and real data examples. In particular, for a recent 4D time-lapse survey, the 4D noise was substantially suppressed when our inversion results were applied.

One limitation of the current inversion method is that constant systematic errors are difficult to detect (Docherty and Hays, 2012). For instance, bulk shifts of node array depth can instead be absorbed into the velocity term. To avoid this issue, other auxiliary measurements such as bathymetry maps of the water bottom can be used for calibration of node depths. Another limitation is that shots located near the acquisition boundaries are not being used for inversion due to lack of near-offset data points and require interpolation/extrapolation from neighboring shots close in time.

Acknowledgements

We thank BP and BHP Billiton for the permission to use the real data examples and CGG for the permission to publish this paper.

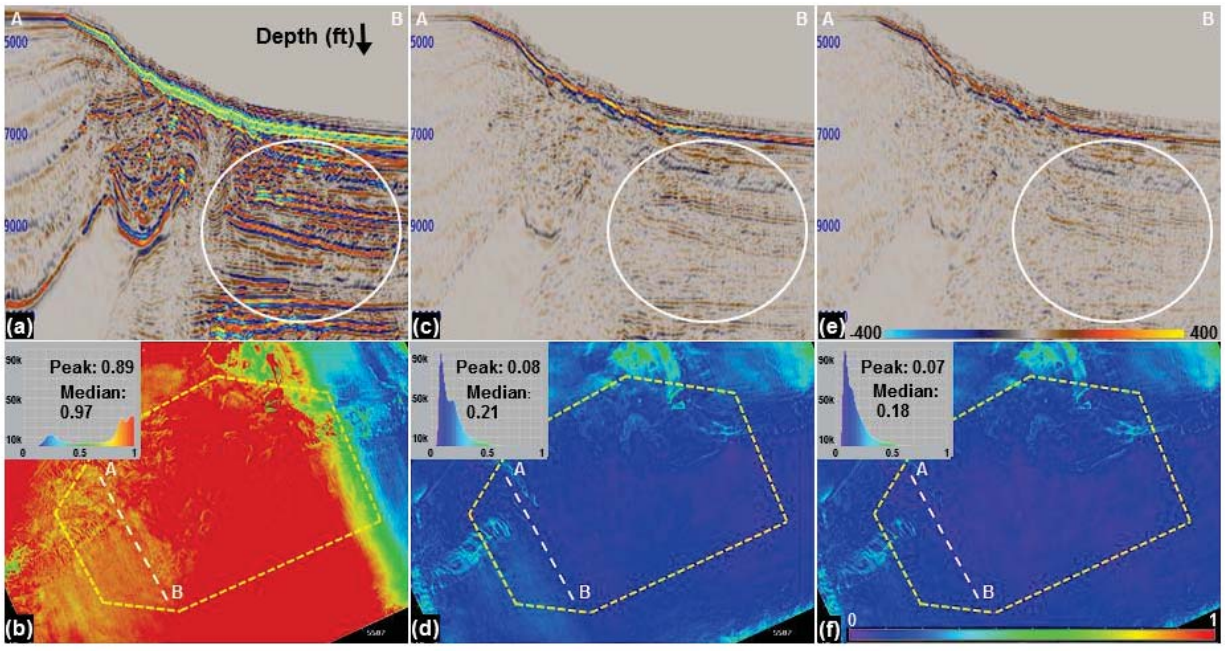

Figure 6: Stacked section of direct difference between baseline and monitor 25 Hz RTM image (top) and the corresponding 4D NRMS extracted from the water bottom (bottom); without inversion (a, b), with inversion excluding node depth inversion (c, d), with inversion including node depth inversion (e, f). Yellow polygon encompasses nodes coverage area and white dashed line shows the location of displayed stacked sections.

© 2016 SEG

Downloaded 09/20/16 to 95.215.237.244. Redistribution subject to SEG license or copyright; see Terms of Use at http://library.seg.org/

EDITED REFERENCES

Note: This reference list is a copyedited version of the reference list submitted by the author. Reference lists for the 2016 SEG Technical Program Expanded Abstracts have been copyedited so that references provided with the online metadata for each paper will achieve a high degree of linking to cited sources that appear on the Web.

REFERENCES

Advocate, D. M., and K. C. Hood, 1993, An empirical time-depth model for calculating water depth northwest Gulf of Mexico: Geo-Marine Letters, **13**, 207–211, http://dx.doi.org/10.1007/BF01207749.

Ahmed, I., B. Nguyen, and M. Roberts, 2013, Joint inversion for ocean bottom node position and average water velocity along shot line: 83rd Annual International Meeting, SEG, Expanded Abstracts, 4880–4884, http://dx.doi.org/10.1190/segam2013-1240.1

Docherty, P. C., and D. Hays, 2012, Ambiguities in direct arrival time inversion for ocean bottom nodes: 74th Annual International Conference and Exhibition, EAGE, Extended Abstracts.

Dosso, S. E., M. R. Fallat, B. J. Sotirin, and J. L. Newton, 1998, Array element localization for horizontal arrays via Occam's inversion: The Journal of the Acoustical Society of America, **104**, 846–859. http://dx.doi.org/10.1121/1.423359.

Hatchell, P., and K. Mehta, 2010, Ocean Bottom Seismic (OBS) timing drift correction using passive seismic data: 80th Annual International Meeting, SEG, Expanded Abstracts, 2054–2058, http://dx.doi.org/10.1190/1.3513249.

Huang, R., P. Wang, K. Nimsaila, and M. Vu, 2016, Angle-dependent water column statics correction through sparse TauP inversion: 78th Annual International Conference and Exhibition, EAGE, Extended Abstracts.

Lecerf, D., A. Lafram, J.-L. Boelle, and J. Cantillo, 2011, Ocean Bottom Node processing in deep offshore environment for reservoir monitoring: 12th International Congress of the Brazilian Geophysical Society and EXPOGEF, 2095–2098.

Olofsson, B., and G. Woje, 2010, Ensuring correct clock timing in ocean bottom node acquisition: 80th Annual International Meeting, SEG, Expanded Abstracts, 172–176, http://dx.doi.org/10.1190/1.3513176.

Peng, X. F., and W. Li, 2010, The alternating-direction iterative method for saddle point problems: Applied Mathematics and Computation, **216**, 1845–1858, http://dx.doi.org/10.1016/j.amc.2009.12.020.

Stopin, A., P. J. Hatchell, C. Corcoran, E. Beal, C. Gutierrez, and G. Soto, 2011, First OBS to OBS time lapse results in the Mars basin: 81st Annual International Meeting, SEG, Expanded Abstracts, 4114–4118, http://dx.doi.org/10.1190/1.3628065.

Undergaard, C., and K. Craft, 2012, Analysis of water column complexity in OBN data: 74th Annual International Conference and Exhibition, EAGE, Extended Abstracts, Paper B046.

Wang, K. L., P. Hatchell, C. Udengaard, K. Craft, and S. Dunn, 2012, Direct measurement of water velocity and tidal variations in marine seismic acquisition: 82nd Annual International Meeting, SEG, Expanded Abstracts, 1–5, http://dx.doi.org/10.1190/segam2012-0806.1.

Zietal, R., and R. Haacke, 2016, Measurement and dynamic wavefield correction for time-dependent water-velocity changes: 78th Annual International Conference and Exhibition, EAGE, Extended Abstracts.

© 2016 SEG